# Molecular Dynamics Simulations and Elastic Network Analysis of Protein Kinase B (Akt/PKB) Inactivation

Shu Cheng and Masha Y. Niv*

Institute of Biochemistry, Food Science and Nutrition, The Robert H. Smith Faculty of Agriculture, Food, and Environment, The Hebrew University, Rehovot 76100, Israel

Received February 23, 2010

Akt (also called protein kinase B−PKB) is a key component of the phosphoinositide-3-kinase signaling pathway, which is responsible for cell proliferation and survival and is a novel target for antioncogenic indications. In its fully activated state, Akt is phosphorylated on the activation loop (A-loop) at residue Thr 309. We used molecular dynamics (MD) simulations and elastic network model normal-mode analysis (ENM-NMA) to study the initial stages of the active−inactive transition in the kinase catalytic domain. We first carried out MD simulations of the active phosphorylated Akt in complex with its ligands under different protonation states of His 196, the phosphothreonine-coordinating residue found in the αC helix. Analysis of trajectories suggested that the doubly protonated His 196 is most compatible with the crystallographic structure. Next we studied the dynamic processes involved in Akt inactivation: detachment of the ligands and A-loop dephosphorylation resulted in MD trajectories with increased mobility, particularly in the N-lobe and in the HJ-αG region of the C-lobe, and in stronger correlation and anticorrelation of motions. The first principal motions derived from the trajectories of phosphorylated and dephosphorylated apo structures were similar to each other but differed from the first principal motions derived from the complex trajectory. A rather large number of principal components obtained from MD trajectories and of ENM-NMA modes is required to describe the active−inactive conformational change of the kinase. The results are discussed in the context of related computational studies of kinase dynamics and kinase-specific inhibitor design.

## INTRODUCTION

Aberrations in cellular signaling pathways that involve the enzyme Akt (also called protein kinase B−PKB) are implicated in diverse diseases, including cancer, diabetes, and neurodegenerative disorders. Proteins involved in Akt activation and signaling are therefore potential targets for therapeutic intervention.[1] Drugs directed against some of these targets are now in clinical trials for the treatment of several cancers, and the inhibition of Akt activation and signaling remains a major goal of drug discovery.[2,3]

Various novel approaches have been taken to enable the design of selective inhibitors of protein kinases. These include designing peptides that mimic selectivity determining regions in the kinase catalytic domain,[4−6] substrate mimetics,[7,8] inhibition via the regulatory domains[2,9] and irreversible binding to the catalytic domain cysteine.[10] One important approach is to target the inactive conformation of the kinase, as exemplified by the FDA-approved drugs imatinib, nilotinib, and sorafenib.[11]

Akt is a serine/threonine kinase that belongs to the AGC family of kinases,[12] and its catalytic domain shares high similarity with those of protein kinase A (PKA) and protein kinase C (PKC). Akt activation is thought to proceed through recruitment to the membrane via interaction of its PH domain with the phosphoinositides produced by phosphoinositide-3-kinase. The lipid-bound Akt is then phosphorylated by 3-phosphoinositide-dependent protein kinase 1 (PDK1). The functionally independent behaviors of the PH and kinase domains of Akt have been well characterized, and the structures of both have been solved separately.[13]

The kinase domain consists of two lobes, the N-terminal small lobe (N-lobe) and the C-terminal large lobe (C-lobe), shown in Figure 1. The N-lobe harbors the phosphate-binding loop, called the P- or G-loop, which contains a conserved glycine-rich sequence motif (GXGX$\varphi$G). The activation segment (A segment) of the kinase is found in the C-lobe, adjacent to the ATP-binding site, and contains important catalytic elements, such as the DFG (Asp−Phe−Gly) motif. The DFG motif positions ATP for phosphoryl transfer and changes the conformation from the active "DFG-in" to the inactive "DFG-out" form. The activation segment is connected to the N-lobe through the αC helix. In Akt, as in most kinases, the central region of the activation segment, the activation loop (A-loop), harbors a primary phosphorylation site (Thr 309) necessary for activation, which is located close to the magnesium-binding loop, the N terminus of the αC helix and a conserved His/Tyr−Arg−Asp (H/YRD) motif in the catalytic loop. Additional phosphorylation sites, in the C-terminal hydrophobic motif (HM) and the turn motif,[14] have been characterized as well.[12]

Structural analysis of kinase catalytic domains has underscored the fact that different kinases adopt strikingly similar structures when they are active.[15,16] Hydrophobic "spines" that traverse both lobes of the protein kinase molecule and stabilize its active conformation were identified by Kornev and co-workers.[17,18] In contrast, inactive kinases have diverse structures, since there are many ways to disrupt the arrange-

* Corresponding author. E-mail: niv@agri.huji.ac.il. Telephone: 972-8-9489664.

10.1021/ci100076j 
Published on Web 08/24/2010

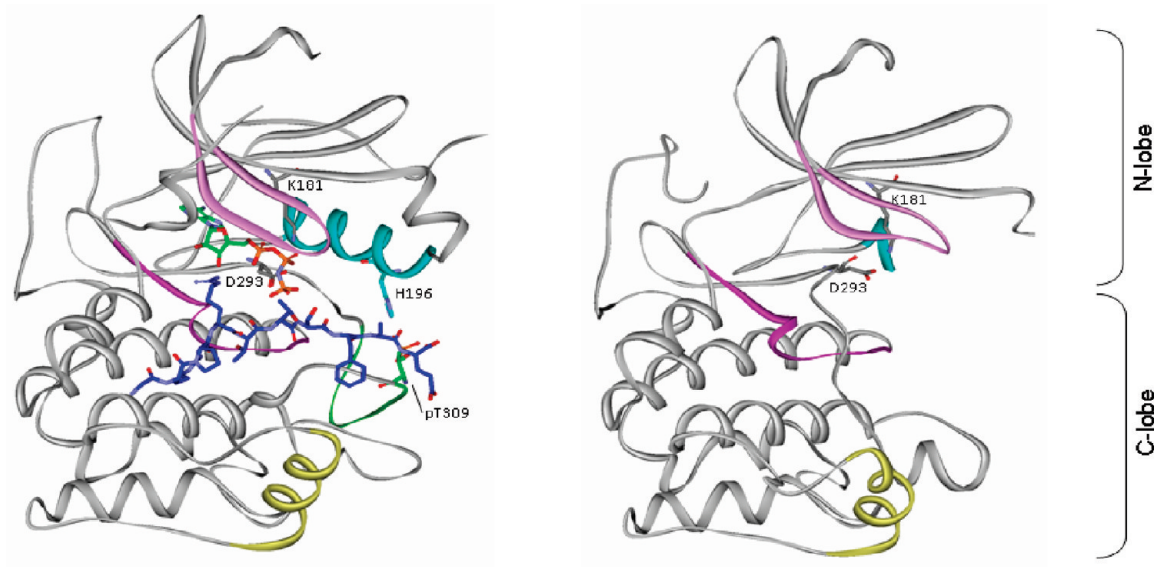


**Figure 1.** Active (left, 1O6K) and inactive (right, 1MRY) structures of Akt. The G-loop (residues 156−167, pink), αC helix (residues 194−206, cyan), catalytic loop (residues 271−283, magenta), A-loop (residues 300−309, green), and αG helix (residues 355−365, yellow) as well as the Mn ions, ANP, and peptide substrate (sticks) are shown. Binding site Lys 181, DFG Asp 293, His 196, and pThr 309 are shown and labeled. Note that parts of the structure are not resolved in the inactive form. The partition to N- and C-lobe is shown schematically on the right.

ment of catalytic residues or to prevent substrate binding. In particular, structures of inactive AGC kinases have revealed a wide range of conformations.[12] Since structural features that are unique to a particular kinase are useful in the design of selective inhibitors,[19] methods for predicting kinase conformations are extremely important.[15,16]

Computational studies are being increasingly applied to elucidate the pathways connecting the active and inactive forms of the kinase catalytic domain. Activation of Src tyrosine kinase was studied using an ensemble of unbiased trajectories to progressively refine and determine the optimal free energy path between two stable conformations. The path was characterized by two main steps in which the A-loop opens first, followed by rotation of the αC helix.[20] Similarly, targeted molecular dynamics (TMD) simulations of c-Kit showed a rapid departure of the juxtamembrane region from the allosteric binding site, followed by a conformational flip of the A-loop from inactive to active conformation and a change in αC helix orientation.[21] TMD of the epidermal growth factor receptor (EGFR) kinase domain suggested a possible pathway for the formation of a stabilizing cluster (spine) during the activation transition.[22] Assembly of the hydrophobic spine, formation of the Src-like intermediate structure, and a cooperative breakage and formation of characteristic salt bridges were proposed as distinct stages in the transition to the active kinase forms of EGFR and Abl.[23]

The backward "active-to-inactive" movement of cyclin-dependent kinase 5 has been recently studied using a metadynamics sampling approach, suggesting a two-step mechanism in which the αC helix rotates by 45° followed by A-loop refolding.[24] Inactivation simulations of Abl indicate significant twisting and hinge-opening motions of the N-lobe with respect to the C-lobe and further outward displacement of the αC helix, leading to an αC-out conformation.[25] Similarly, biased molecular dynamics (MD) of inactivation of the Src family kinase Lyn showed that lobe opening is a simple motion, whereas movement of the A-loop is more complex, requiring secondary structural changes as well as communication with the αC helix. The conformational transition involves a switch in an electrostatic network of six polar residues between the active and down-regulated conformations.[26]

MD simulations and principal component analysis (PCA) of the PKA domain suggest that the most significant motion of the wild-type PKA in the context of a PKA−substrate complex is a "breathing mode", with the two domains of the protein moving in opposite directions around the "hinge" region. The second significant internal motion is a mixture of rotation and twisting between the two lobes. The collective motions in the T197A mutant (Thr 197 corresponds to Thr 309 in Akt) were found to be different from the wild type, and the first three principal motions did not include inter-domain twisting.[27]

The activation/inactivation cycle in Akt is a complex, multicomponent process, with many levels of regulation.[9,28] In the current work, we start from the experimental structure[29] of phosphorylated Akt in complex with ATP (modeled on the crystallographic ANP), ions and peptide substrate (jointly referred to as Akt "ligands"), and apply two computational tools, namely, MD simulations and normal-mode analysis (NMA), to investigate how: (i) phosphorylated complex, (ii) apo-phosphorylated, and (iii) apo-dephosphorylated forms of Akt differ in their dynamics. In the dephosphorylated form, we substitute pThr 309 in the active structure of Akt with Thr. With the complex trajectory as a control, our goal was to study the initial stages of Akt inactivation dynamics induced by detachment of the ligands and the phosphate group.

## MATERIALS AND METHODS

**MD Simulations.** Akt in complex with the magnesium ions, ATP and GSK3-derived peptide was based on the X-ray crystal structure of active PKB (1O6K). We used the continuous residues from 146 to 449, while the rest of the

C-terminal part following the unresolved residues was excluded. The crystallographic ANP molecule and Mn ions were replaced with the physiological ATP and the Mg ions.

Three trajectories of the Akt complex, corresponding to the three protonation states of His 196, (i.e., HSD, HSE, and HSP) were carried out. In addition, two apo trajectories, where ions, ATP, and substrate peptide were deleted from the HSP complex were carried out. Phosphothreonine was replaced by threonine for apo T309, as summarized in Table 1.

All simulations were run in CHARMM.[30] The kinase catalytic domain was solvated within a 47 Å radius water sphere under stochastic boundary conditions and a short energy minimization using the steepest-descent algorithm was performed to remove unfavorable contacts. Nonbonded van der Waals interactions were treated by using a switching function at 12 Å and by reaching zero at a distance of 16 Å. The integration time step was set to 2 fs, and the miscellaneous mean field potential (MMFP) method was used to set up a spherical boundary potential. MD simulation started with 20 ps heating from 100 to 300 K, followed by 180 ps equilibration. The MD was then run for 20 ns with different random initial velocities for different structures, using a CHARMM27 force field, TIP3P explicit water model, and phosphothreonine patch THP2 for pThr 309.

**Computational Estimation of the p$K_a$ of His 196.** We used the H++,[31] Accelrys,[32] and PDB2PQR[33] programs to calculate the p*K*a of His 196 of the active Akt structure (1O6K), where pThr 309 was replaced by Glu 309, returning the values of 12.4, 11.2, and 5.3, respectively (the first two values corresponding to doubly protonated His in physiological pH).

**Covariance Matrix Calculation from MD Trajectories.** The calculations were performed using the CARMA package.[34] The covariance matrix between residues (represented by the $C_\alpha$ atoms) $i$ and $j$ was calculated for each of the 20 ns MD simulation trajectories: snapshots from trajectories were taken every 10 ps, overall translation and rotation were removed, and only $C_\alpha$ was kept for analysis.

$$\mathrm{Cov}(i,j) = \langle \delta\vec{r}_i \cdot \delta\vec{r}_j \rangle = \langle (\vec{r}_i(t) - \langle \vec{r}_i \rangle) \cdot (\vec{r}_j(t) - \langle \vec{r}_j \rangle) \rangle = \frac{1}{K_{\mathrm{frames}}} \sum_{k=1}^{K_{\mathrm{frames}}} \sum_{\chi=1}^{3} (r_{i,\chi}(k) - \bar{r}_{i,\chi})(r_{j,\chi}(k) - \bar{r}_{j,\chi}) \quad (1)$$

where $r_{i,\chi} = x_i, y_i, z_i$ are Cartesian coordinates of the $C_\alpha$ atom of residues $i$ and $\bar{r}_{i,\chi} = (1/K_{\mathrm{frames}})\sum_{k=1}^{K_{\mathrm{frames}}} r_{i,\chi}(k)$. Here $K_{\mathrm{frames}}$ is the number of structures, and $\bar{r}_{i,\chi}$ is an averaged value over all frames in each MD trajectory. The correlation value is the normalized covariance matrix, ranging from −1 to 1.

**PCA to Represent Essential Dynamics of the Trajectory.** To obtain collective motion coordinates that represent the overall dynamics of each trajectory, PCA was performed, in which the covariance matrix, calculated as described above, was diagonalized to yield a set of eigenvectors and eigenvalues. The first eigenvectors, with the largest eigenvalues, capture the predominant motions of the total observed variance. The analysis, including the diagonalization, was performed using the CARMA package.[34]

**NMA-Derived Calculation of Inter-Residue Correlation.** NMA is an approximate but powerful tool to estimate dynamics based on structure.[35] Following our previous work,[36,37] we used an elastic network model (ENM), in which the forces between $C_\alpha$ atoms are described as simple Hookean potentials dependent on distance only. The eigenvalues $\Omega_n$ and eigenvectors $p_n$ are obtained by diagonalizing the ENM-derived Hessian via the NomadRef server,[38] while $p_{n,i,\chi} = x_i, y_i, z_i$ are Cartesian displacements of the $C_\alpha$ atom of residue $i$ in mode $n$.

Correlation between residues $i$ and $j$ was calculated as the average correlation summed over 100 lowest-frequency nontrivial normal modes[39,40]

$$C_{ij} = \frac{\sum_{l=7}^{106} \sum_{\chi=1}^{3} \frac{p_{l,i,\chi} p_{l,j,\chi}}{\Omega_l}}{\left( \sum_{m=7}^{106} \sum_{\chi=1}^{3} \frac{(p_{m,i,\chi})^2}{\Omega_m} \right)^{1/2} \left( \sum_{n=7}^{106} \sum_{\chi=1}^{3} \frac{(p_{n,j,\chi})^2}{\Omega_n} \right)^{1/2}} \quad (2)$$

which was enough for convergence of the correlation matrix (results not shown). The calculation was performed for $C_\alpha$ atoms of Akt with and without the peptide. The ATP and the phosphorylation state are not accounted for in the $C_\alpha$ level of treatment.

**Comparison with Deformation Vector.** The missing residues of the inactive Akt were predicted using Modloop[41] or SuperLooper.[42] The degree of similarity or squared overlap between normal mode $m$ (or the direction of a normalized eigenvector from PCA) and normalized deformation vector is calculated as

$$I_m^2 = \sum_{i=1}^{3N} (p_{mi} \Delta x_i)^2 \quad (3)$$

where $N$ is the number of $C_\alpha$ atoms included in the structures. The cumulative overlap is defined as the sum of squared overlaps between the deformation vector and normal mode 1, 2, and so on. It reaches the value of "1" when all squared overlaps with all $3N$ eigenvectors (which represent an orthogonal spanning basis set for the system) are summed.

**Table 1.** Summary of Trajectories

| name of trajectory | components | H196 protonation | T309 state |
|---|---|---|---|
| complex | Akt, peptide, ions and ATP in water | HSP | phosphorylated |
| HSD | Akt, peptide, ions and ATP in water | HSD | phosphorylated |
| HSE | Akt, peptide, ions and ATP in water | HSE | phosphorylated |
| apo pT309 | Akt in water | HSP | phosphorylated |
| apo T309 | Akt in water | HSP | unphosphorylated |

## RESULTS AND DISCUSSION

**Summary of Systems Studied.** To investigate the initiation of inactivation dynamics of Akt, several explicit model simulations were carried out, as detailed in Table 1.

**Doubly Protonated State of His 196 Is in Agreement with the Complex Structure.** One of the challenges in MD simulations is to correctly assign the residues protonation states. The computational prediction of the p$K_a$ and thus of the protonation state of His residues is particularly challenging.[33,43] His 196 coordinates pThr 309 in the A-loop, and we therefore assumed that its protonation state might influence the local and global features of Akt dynamics. The

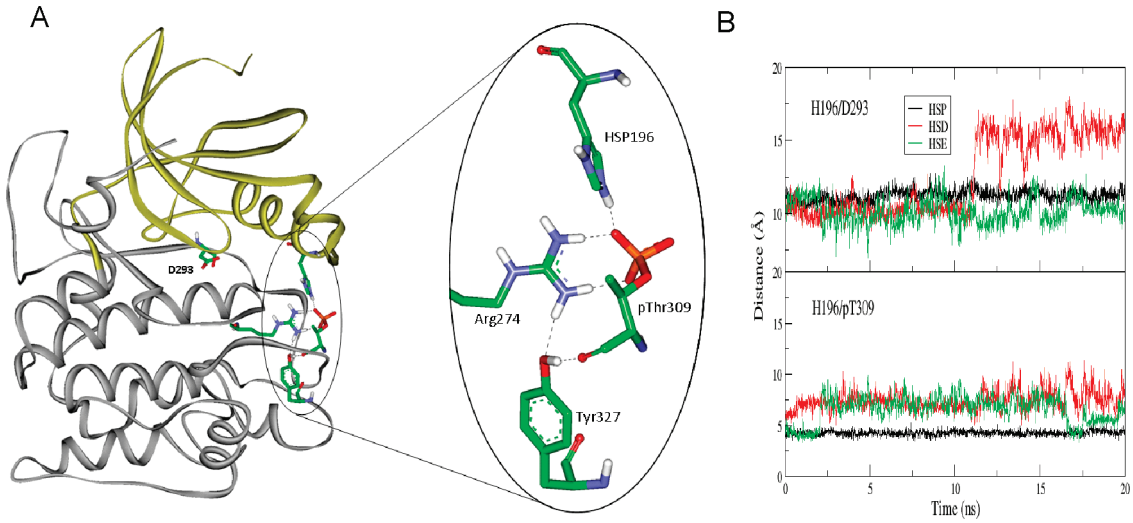


**Figure 2.** Residues stabilizing pThr309 in the Akt complex. (A) Representative illustration of pT309-binding residues (colored by atom type) and hydrogen bonds (shown by dotted gray lines) of Akt complex with His 196 in the doubly protonated state. The phosphate group on T309 is shown in orange. The N- (residues 146−235) and the C-lobes (residues 236−449) are shown in gold and gray ribbons, respectively. (B) The shortest heavy-atom distances of the two residue pairs H196/D293 and H196/pT309 are calculated for Akt complex, with three protonation states of His 196, i.e., HSP, HSD, and HSE (black, red, and green lines, respectively).

important roles of the equivalent His 87 in PKA[44−46] and Arg 96 in GSK3$\beta$[47] have been previously highlighted. The protonation state of His 196 is predicted to be doubly protonated (HSP),[31,32] but other protonation states have been suggested as well.[27,33] We therefore first performed 20 ns MD simulations of the Akt complexed with its ligands,[29] applying all three possible protonation states of His 196, i.e., singly protonated on the $\delta$ nitrogen (HSD) or $\epsilon$ nitrogen (HSE) and doubly protonated (HSP). These and the rest of the simulations carried out in the current work are detailed in Table 1.

Distances of His 196 from other residues in its vicinity (see Figure 2A) are stable in the HSP trajectory but fluctuate in the singly protonated trajectories. For example, the H196/D293 distance, which is indicative of the motion of the DFG motif (C-lobe) relative to the αC helix (N-lobe), and the H196/pT309 pair, which monitors the distance between the A-loop (C-lobe) and αC helix (N-lobe), are shown in Figure 2B. HSD and HSE 196, but not HSP, move more than 6 Å away from the phosphate group of pThr 309. Hence, the dynamics of complexes HSD and HSE suggest deviation from the active conformation of the kinase as captured in the crystal structure. We thus concluded that the doubly protonated state of HSP 196 is the correct form at physiological pH, and this protonation state was used in further apo simulations.

**Lobe Uncoupling Occurs in the Apo Trajectories.** The conformation of the activated Akt, phosphorylated on the A-loop, differs markedly from its inactive counterpart (Figure 1), which is characterized by a disordered αC helix, A-loop, and HM[48] and in which the N terminus of the αG helix is somewhat deformed.

To begin elucidating the process of inactivation, we performed simulations of two initial structures: an apo pT309 (chain A in 1O6K) and the same monomer with the phosphate detached from Thr 309, apo T309 (see Table 1 for summary of trajectories). The short distance between His 196 and residue 309 (4.25 Å in the active crystal structure) quickly lengthens in the MD simulations of both apo pT309 and T309 forms, reaching up to 10 Å (Figure 3). This is in agreement with a PKA study in which formation of the equivalent H87/T197 pair was shown to be less likely in the absence of contacts with the ATP ligand.[46] The result suggests that the interactions between the two lobes loosen in the absence of ligands. The uncoupled H196/T309 fluctuations may reflect the intrinsic dynamics of Akt.

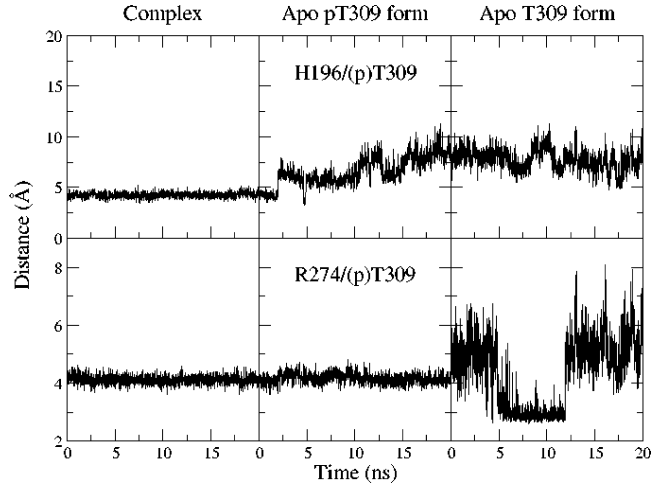


**Figure 3.** The shortest heavy-atom distances of the two residue pairs H196/(p)T309 and R274/(p)T309 are calculated for the complex (left), the apo pT309 (middle) and T309 (right) forms. Salt bridges link the A-loop residue pThr 309 with the catalytic loop residue Arg 274 from the H/YRD motif. This interaction is maintained in the complex and apo pT309 trajectories and explains the tight coupling of the A- and C-loops in the phosphorylated form of kinases. In the apo Thr 309 form, the stabilizing network is severed due to detachment of the phosphate group. Figure 3 shows the distance between Thr 309 and Arg 274. As expected, there are much larger fluctuations and generally longer distances in the apo T309 trajectory compared to that of the apo pT309 and complex trajectories, indicating a loss of coupling between the A- and C-loops in the 20 ns following dephosphorylation.

Interestingly, both Arg 274 and Thr 309 maintain a hydrogen bond with Tyr 327 (Figure 2A) during the simulated time scale in both phosphorylated and unphos-

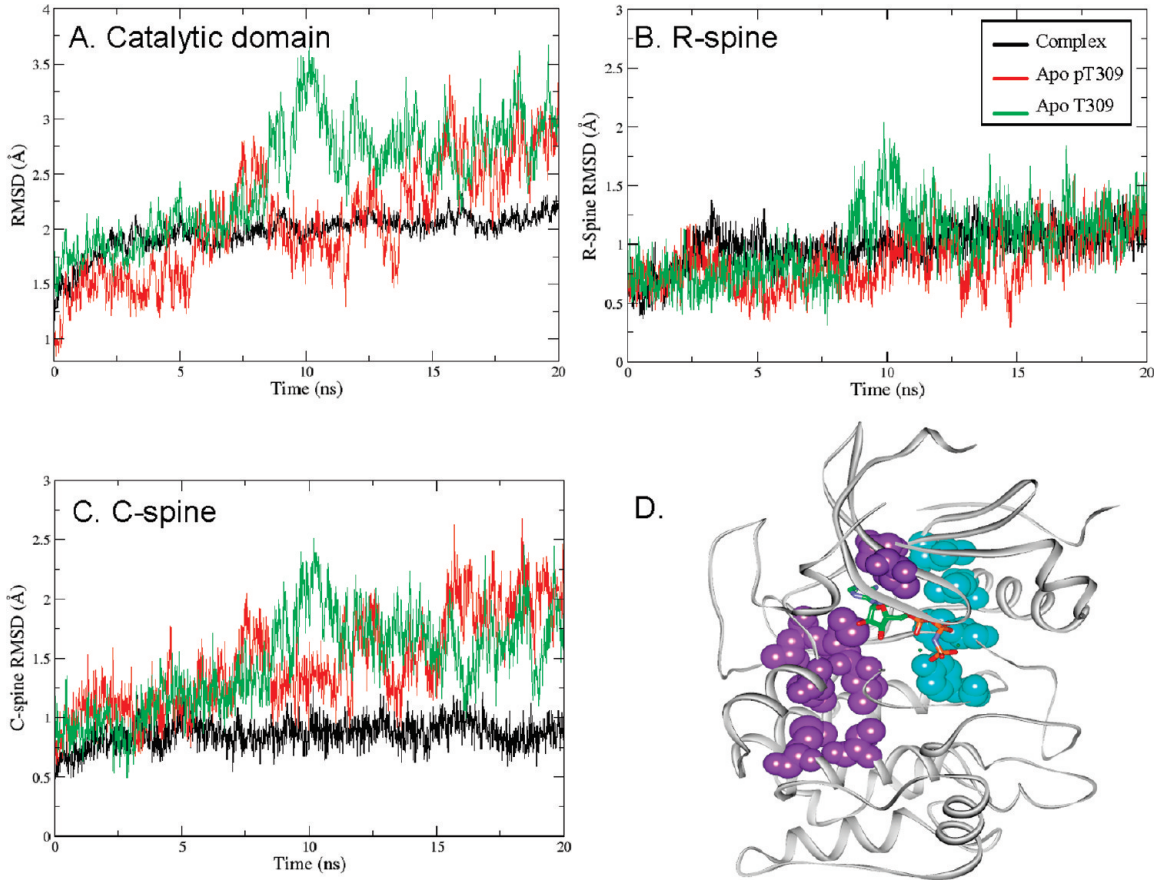


**Figure 4.** Backbone RMSD for the complex (black), apo pT309 (red) and T309 (green) trajectories, calculated for the (A) catalytic domain, and the (B) R- and (C) C-spine residues. (D) Sphere representation of the C- (violet, on the left) and R-spines (cyan, on the right).

phorylated apo trajectories (data not shown). This residue, corresponding to Tyr 215 in PKA, is conserved in the AGC kinases.

**Apo Trajectories Present Larger Deviations from the Initial Structure than the Complex.** Root-mean-square deviations (RMSD) of the catalytic domain backbone atoms during the 20 ns MD simulations of the complex, apo pT309 and T309 trajectories are plotted in Figure 4A. As expected, the most stable trajectory is of the complex Akt, while RMSD increases in the apo pT309 trajectory and even more so in the apo T309 trajectory. The complex trajectory reached reasonable equilibration within 2.5 ns, whereas RMSD continued to rise for the perturbed apo trajectories. Dephosphorylation induced a rapid deviation from the initial crystal structure.

The trajectories were next analyzed in terms of the hydrophobic "spines".[17,18] The "regulatory spine" (R-spine) corresponds to residues L204, L215, Y273, and F294 in Akt. The "catalytic spine" (C-spine) corresponds to residues V166, A179, L237, L281, M282, L283, V339, and M343 in Akt and is completed by the adenine ring of ATP. The R-spine remained almost intact in all the trajectories (Figure 4B), while the C-spine in the apo trajectories began to deteriorate promptly upon ligand and phosphate-group detachment (Figure 4C), reaching a value close to the RMSD of the inactive (1MRY) C-spine from the active (1O6K) spine, around 1.8 Å. The increase in the C-spine RMSD is mostly due to increased N-lobe mobility (see below), leading to interlobe opening.

The root-mean-square fluctuations (RMSF) of $C_\alpha$ atoms in each residue are presented in Figure 5. Overall, the N-lobe

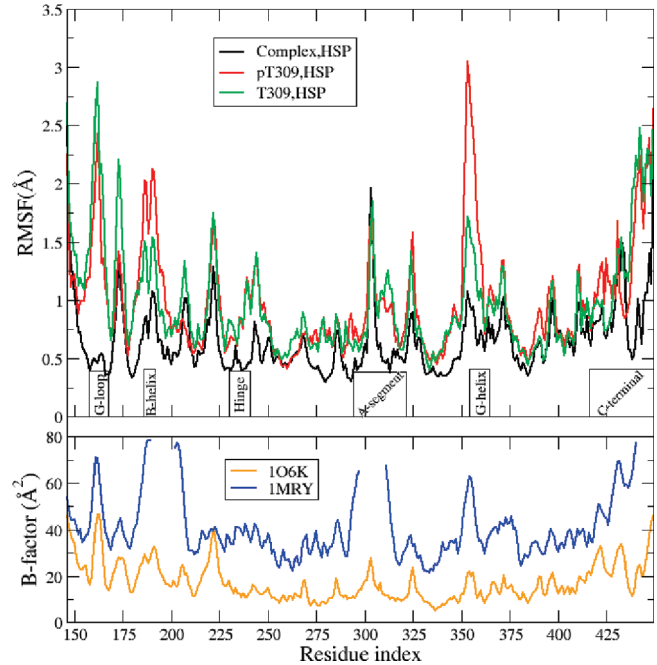


**Figure 5.** RMSF of $C_\alpha$ atoms (top) and B-factors for active (1O6K) and inactive (1MRY) crystal structures (bottom).

becomes more mobile upon ligand and phosphate detachment. Particularly flexible regions for the two apo structures were identified: the G-loop and αB helix in the N-lobe, the C-terminal part of the activation segment, and the loop connecting the αF (residues 331−345) and αG (residues 355−365) with the N terminus of the αG helix (also called

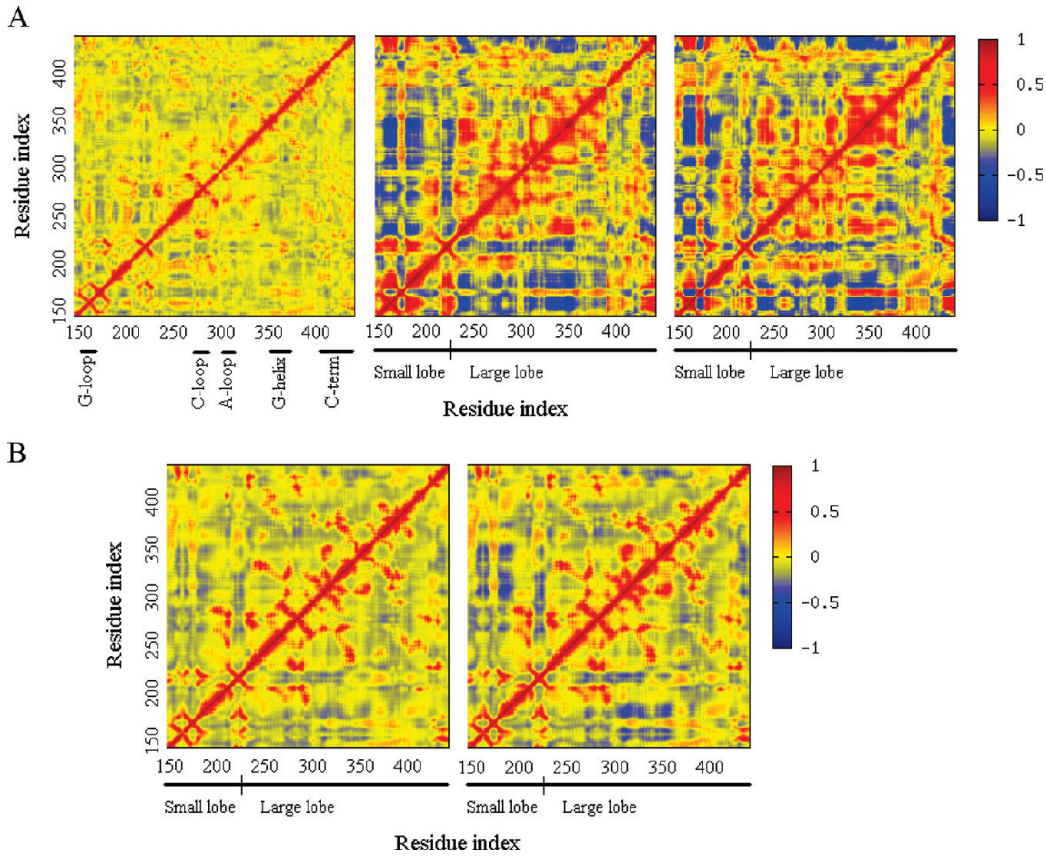


**Figure 6.** Covariation of motion calculated from the MD trajectories and using ENM−NMA. (A) Calculated normalized covariance matrix of the 20 ns MD trajectories for the complete Akt structure of the complex (left) and the apo pT309 (middle) and T309 (right) forms. Five key domains of G-, C-, and A-loops, αG helix, and C-terminus are labeled on the left map. (B) Correlation calculated from the nonzero 100 lowest-frequency normal modes of Akt with (left) and without (right) the peptide.

the HJ−αG region),[4] the C-terminal tail and the hinge between the lobes. These structural elements are stabilized in the Akt complex, and most of them are involved in ligand (ATP and substrate) binding. The largest fluctuation is in the αG helix in the apo-phosphorylated trajectory and in the G-loop in the apo-dephosphorylated trajectory, with smaller changes in the activation (A) loop. The flexibility of the HJ substrate-binding region had been observed in our previous study[37] and may be related to transformation of the N-terminus of the αG helix into a slightly deformed helix in the inactive crystal structure of Akt. In general, the identified flexible regions have a very high B-factor in the inactive structure (1MRY)[48] (Figure 5) and are in overall agreement with a normal mode-based flexibility analysis performed on a set of Ser/Thr and Tyr active and inactive apo structures of protein kinase domains.[37]

**Correlation and Anticorrelation of Motions, Calculated by either MD or NMA, Increase in the Apo States.** To further explore the initialization of the inactivation dynamics, the covariance matrix between residues represented by their $C_\alpha$ atoms was calculated for 20 ns MD trajectories. It is evident from the three covariance maps (Figure 6A) that the apo trajectories differ markedly from the complex trajectory and display increased levels of motional correlation (red) and anticorrelation (blue). This is consistent with the fluctuations calculated for PKA which demonstrated that the amplitude of the correlation between several loops is large for the ligand-free structure.[46]

An efficient and computationally simple approach to studying molecular motions is NMA, in which molecular motions are decomposed into orthogonal vectors representing vibrational motions (normal modes). In the ENM version of the NMA used here, a harmonic potential with a single force constant accounts for pairwise interactions between all $C_\alpha$ atoms that are within a certain cutoff distance.[38] The NMA-derived correlations calculated for the complex and for the apo structures are shown in Figure 6B. The phosphorylation and the presence of ATP are not represented at the Cα-based NMA level of treatment adopted here, but the effect of substrate peptide on the correlation within the catalytic kinase domain could be assessed. The overall similarity between the NMA- and MD-derived correlations and the trend of increased anticorrelated motions in the apo state compared to the complex state are apparent in Figure 6.

**First MD-Derived Principal Component Is Similar for the Apo Trajectories but Not the Complex Trajectory.** To reduce the dimensional space of the data sets from MD trajectories and highlight the principal motions of ligand detachment and dephosphorylation-induced dynamics, PCA was performed, in which the covariance matrix was diagonalized to yield a set of eigenvectors and eigenvalues. The eigenvectors represent the directions in a multidimensional space, describing independent modes of atomic motion, while the eigenvalues represent their corresponding amplitudes.[49,50] The first few PC modes characterize the dominant motions of PKB in each MD trajectory.

Figure 7A shows that ligand detachment induces a pronounced motion, most dramatically of the N-lobe. While in the complex trajectory PC1 is dominated by the motion of the C- and N-terminal tails, in apo pT309, PC1 can be

A

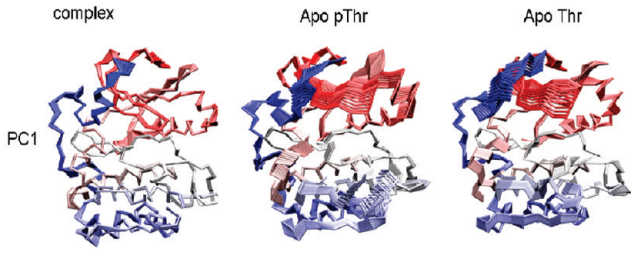


B

| Cosine product | PC1 (complex) | PC1 (Apo pT) | PC1 (Apo) |
|---|---|---|---|
| PC1 (complex) | 1 | 0.04 | 0.12 |
| PC1 (Apo pT) | | 1 | 0.75 |
| PC1 (Apo) | | | 1 |

**Figure 7.** (A) Illustrative conformations along PC1 of the three different trajectories are shown. The protein is represented by trace and colored according to residue numbering, starting with red in the N-term and finishing with blue in the C-term (prepared in VMD).[51] (B) Overlaps of PC1 from different trajectories.

described as a breathing mode in which the G-loop and αC helix move together against the HJ−αG region of the C-lobe. Similar motion has been found in PKA.[27] High-displacement regions in PC1 (Figure 7A) as well as in PC2 (Supporting Information, Figure S1) correspond to the high-RMSF regions (Figure 5), with the N-lobe and the αG region in the C-lobe exhibiting pronounced dynamics in the apo trajectories.

To compare the essential dynamics in the three trajectories, we calculated the inner products between the first eigenvectors from each trajectory (Figure 7B). The overlap values between PC1 from the complex and the apo trajectories are small, while PC1 of both apo pT309 and T309 have overlaps reaching as high as 0.75. The results indicate that the apo trajectories are more similar to each other than to the complex trajectory. This means that, on the time scale of our simulations, the ligand-detachment-induced conformational changes play a dominant role in Thr 309 dephosphorylation.

**Deformation Vector Is Not Dominated by a Few PC or Normal Mode Vectors.** A change from one conformation of a protein to another is often called the "deformation vector", $\Delta \boldsymbol{x}$, and corresponds to the normalized atomic displacement between the initial and final conformation (computed as the difference in atomic coordinates after superimposition of the structures). The overlap between a collective motion (described by either PC or normal mode) and the deformation vector indicates the similarity of the atomic displacement in that mode and the overall conformational change between the initial and final states. If the overlap equals "1", then the conformational change is fully described by a single collective mode. Cumulative overlap represents the sum of individual squared overlaps, starting from the lowest nonzero frequency modes. It has been previously shown that a conformational change between two states can be described by a linear combination of a few low-frequency normal modes in many[36,52] but not all cases.[53,54] Here we describe a transformation involved in the transition from active to inactive conformation in terms of PC vectors and normal modes. We calculated the overlap between the deformation vector $\Delta \boldsymbol{x}$, defined by the difference

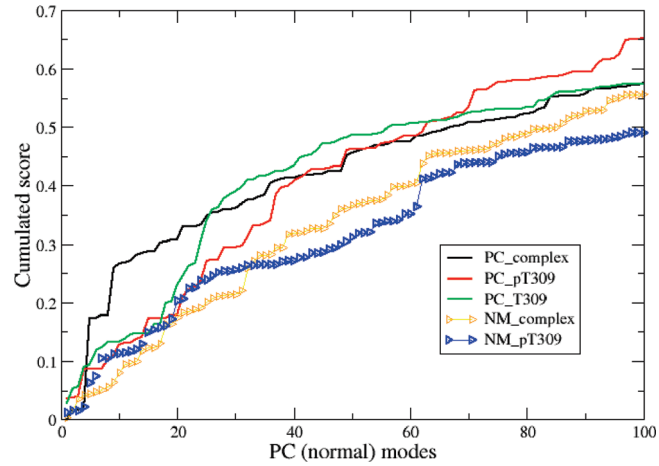


**Figure 8.** Cumulative contributions of principal components and normal modes to the active−inactive conformational change.

in the $C_\alpha$ atom positions in the active and inactive crystal structures of Akt and the $n$th eigenvector from PCA or NMA. Figure 8 presents the cumulative values for up to 100 first eigenvectors obtained from the Akt complex and the apo trajectories as well as for the 100 lowest-frequency normal modes obtained by means of the ENM from the initial structure of the complex and apo forms. Over 50 vectors are needed to describe 50% of the conformational change. The reason that the active−inactive transition of a protein kinase could not be described by a few low-frequency modes is due to the rather complex changes, including those in the A-loop, that are involved in the transition. In a recent study of active−inactive transition in CDK kinase, the authors concluded that the N-lobe has the intrinsic ability to move toward the bound conformations, whereas the activation loop does not have such an intrinsic, structure-encoded ability.[55]

Interestingly, a comparable number of eigenvectors from PCA and NMA is needed to reach the cumulative sum of overlaps with the deformation vector. The results are robust with respect to different loop predictions of the inactive structure (results not shown). Furthermore, cumulative overlaps for the conformational transition of CDK2 (1HCL to 1FIN, no residues missing) were similar: about 100 normal modes were needed to describe close to 50% of the change (Supporting Information, Figure S2).

On the simulated time scale, we did not see a significant difference between PCs derived from the different trajectories in terms of their ability to describe the active−inactive transition. Longer time-scale simulations of the apo structures are planned in order to identify the time frames within which the R-spine disassembles and the overlap with the deformation vector increases. It would be interesting to see whether a significant increase in the simulation time of the dephosphorylated apo form (en route to inactivation) results in PCA modes that better describe the inactivation conformational change compared to a similar simulation of the phosphorylated apo form.

## CONCLUSIONS

The emerging consensus from computational studies of kinase activation/inactivation dynamics is that during the inactive−active transition, the A-loop opens first, followed by rotation of the αC helix, while in the active−inactive

transition, the interlobe opening and αC helix rotation are followed by A-loop refolding. This notion is supported in the current study, in which the N-lobe motion and the outward motion of αC were observed in the root-mean-square fluctuations (RMSF) and the essential dynamics components, while only small changes were observed in the A-loop.

We found that on a 20 ns time scale, the interactions between the two lobes loosen upon ligand detachment independently of Thr 309 dephosphorylation, while the tight coupling of the A- and C-loops is present in the phosphorylated, but not in the unphosphorylated, form. The R-spine is kept almost intact in the apo trajectories, while the C-spine begins to deteriorate promptly upon ligand detachment. We did not observe a flip in the DFG conformation, consistent with the absence of any observed flip in longer 100−300 ns simulations of Abl inactivation.[25] Indeed, NMR studies of p38 and PKA kinases suggest $\mu$s to ms scale DFG motions.[25] The abundant ATP-competitive inhibitors (called type 1) recognize the active "DFG-in" conformation found in most of the X-ray structures, while type 2 kinase inhibitors recognize the inactive "DFG-out" conformation of the kinase.[11,56] In a practical and successful approach to facilitating type 2 inhibitor design when inactive structures are unavailable by modulating the available "DFG-in" structures, DOLPHIN (deletion-of-loop Asp−Phe−Gly-in) was introduced.[57] Efforts continue to extend simulations of dynamics to the relevant time scales,[25,58] where one of the motivations is a future ability to target an intermediate conformation.

Part of the kinase conformational space can be spanned by normal modes of a single structure, and inclusion of normal mode-based descriptions of protein flexibility was shown to improve computational docking of small molecules to proteins kinases.[55,59−61] However, it has been also shown that the A-loop dynamics cannot be accounted for by a simple combination of a few modes.[55] This was reconfirmed here by both the elastic network normal modes and principal components obtained from 20 ns long atomistic simulations.

It would be interesting to see whether a more efficient description can be obtained by principal component analysis (PCA) from longer simulations. To extend accessible simulation time scales, we are developing a method for the structural decomposition of kinases into rigid blocks and flexible regions[37] to be used in conjunction with the accelerated dynamics methods, such as rotation and translation block (RTB) dynamics.[62,63]

Our study shows that different protonation states can significantly influence the conformational dynamics of the kinase. The protonation state of the catalytically important aspartate[25,64] and the role of pH dependence and titratable residues in determining kinase activity levels have been studied.[44] Further combinations of computation and experimentation are likely to shed more light on the relationships between phosphorylation and pH.

## ACKNOWLEDGMENT

We thank Anat Levit for valuable help and critical reading of the manuscript, Prof. Rob Coalson, Marina Shudler, and Inbal Sela for discussions, and the anonymous reviewers for important critique. This work was funded by the U.S.−Israel Binational Science Foundation grant no. 2007296.

**Supporting Information Available:** Two figures (Figures S1: square displacement of $C_\alpha$ atoms along PC1 and PC2 and S2: cumulative contribution of normal modes of CDK2 to active−inactive transformation). Movies of PC1 and PC2 and nontrivial normal modes 1 and 2 of the complex and apo trajectory were prepared with the UCSF Chimera package[65] from the Resource for Biocomputing, Visualization, and Informatics at the University of California, San Francisco (supported by NIH P41 RR-01081). This information is available free of charge via the Internet at http://pubs.acs.org/.

## REFERENCES AND NOTES

(1) Restuccia, D. F.; Hemmings, B. A. Blocking Akt-ivity. *Science* **2009**, *325*, 1083–1084.
(2) Lindsley, C. W.; Barnett, S. F.; Layton, M. E.; Bilodeau, M. T. The PI3K/Akt pathway: Recent progress in the development of ATP-competitive and allosteric Akt kinase inhibitors. *Curr. Cancer Drug Targets* **2008**, *8*, 7–18.
(3) Klein, S.; Levitzki, A. Targeting the EGFR and the PKB pathway in cancer. *Curr. Opin. Cell Biol.* **2009**, *21*, 185–193.
(4) Niv, M. Y.; Rubin, H.; Cohen, J.; Tsirulnikov, L.; Licht, T.; Peretzman-Shemer, A.; Cna'an, E.; Tartakovsky, A.; Stein, I.; Albeck, S.; Weinstein, I.; Goldenberg-Furmanov, M.; Tobi, D.; Cohen, E.; Laster, M.; Ben-Sasson, S. A.; Reuveni, H. Sequence-based design of kinase inhibitors applicable for therapeutics and target identification. *J. Biol. Chem.* **2004**, *279*, 1242–55.
(5) Mack, E.; Ziv, E.; Reuveni, H.; Kalman, R.; Niv, M. Y.; Jorns, A.; Lenzen, S.; Shafrir, E. Prevention of insulin resistance and beta-cell loss by abrogating PKCepsilon-induced serine phosphorylation of muscle IRS-1 in Psammomys obesus. *Diabetes/Metab. Res. Rev.* **2008**, *24*, 577–84.
(6) Rubinstein, M.; Niv, M. Y. Peptidic modulators of protein-protein interactions: progress and challenges in computational design. *Biopolymers* **2009**, *91*, 505–13.
(7) Litman, P.; Ohne, O.; Ben-Yaakov, S.; Shemesh-Darvish, L.; Yechezkel, T.; Salitra, Y.; Rubnov, S.; Cohen, I.; Senderowitz, H.; Kidron, D.; Livnah, O.; Levitzki, A.; Livnah, N. A novel substrate mimetic inhibitor of PKB/Akt inhibits prostate cancer tumor growth in mice by blocking the PKB pathway. *Biochemistry* **2007**, *46*, 4716–24.
(8) Tal-Gan, Y.; Freeman, N. S.; Klein, S.; Levitzki, A.; Gilon, C. Synthesis and structure-activity relationship studies of peptidomimetic PKB/Akt inhibitors: The significance of backbone interactions. *Bioorg. Med. Chem.* **2010**, *18*, 2976–2985.
(9) Calleja, V.; Laguerre, M.; Parker, P. J.; Larijani, B. Role of a Novel PH-Kinase Domain Interface in PKB/Akt Regulation: Structural Mechanism for Allosteric Inhibition. *PLoS Biol.* **2009**, *7*, 189–200.
(10) Toral-Barza, L.; Zhang, W. G.; Huang, X.; McDonald, L. A.; Salaski, E. J.; Barbieri, L. R.; Ding, W. D.; Krishnamurthy, G.; Hu, Y. B.; Lucas, J.; Bernan, V. S.; Cai, P.; Levin, J. I.; Mansour, T. S.; Gibbons, J. J.; Abraham, R. T.; Yu, K. Discovery of lactoquinomycin and related pyranonaphthoquinones as potent and allosteric inhibitors of AKT/PKB: mechanistic involvement of AKT catalytic activation loop cysteines. *Mol. Cancer Ther.* **2007**, *6*, 3028–3038.
(11) Zhang, J. M.; Yang, P. L.; Gray, N. S. Targeting cancer with small molecule kinase inhibitors. *Nat. Rev. Cancer* **2009**, *9*, 28–39.
(12) Pearce, L. R.; Komander, D.; Alessi, D. R. The nuts and bolts of AGC protein kinases. *Nat. Rev. Mol. Cell Biol.* **2010**, *11*, 9–22.
(13) Calleja, V.; Alcor, D.; Laguerre, M.; Park, J.; Vojnovic, B.; Hemmings, B. A.; Downward, J.; Parker, P. J.; Larijani, B. Intramolecular and intermolecular interactions of protein kinase B define its activation in vivo. *PLoS Biol.* **2007**, *5*, 780–791.
(14) Hauge, C.; Antal, T. L.; Hirschberg, D.; Doehn, U.; Thorup, K.; Idrissova, L.; Hansen, K.; Jensen, O. N.; Jorgensen, T. J.; Biondi, R. M.; Frodin, M. Mechanism for activation of the growth factor-activated AGC kinases by turn motif phosphorylation. *EMBO J.* **2007**, *26*, 2251–2261.
(15) Huse, M.; Kuriyan, J. The conformational plasticity of protein kinases. *Cell* **2002**, *109*, 275–82.
(16) Jacobs, M. D.; Caron, P. R.; Hare, B. J. Classifying protein kinase structures guides use of ligand-selectivity profiles to predict inactive conformations: Structure of lck/imatinib complex. *Proteins* **2008**, *70*, 1451–1460.
(17) Kornev, A. P.; Haste, N. M.; Taylor, S. S.; Eyck, L. F. Surface comparison of active and inactive protein kinases identifies a conserved activation mechanism. *Proc. Natl. Acad. Sci. U.S.A.* **2006**, *103*, 17783–17788.

(18) Kornev, A. P.; Taylor, S. S. Defining the conserved internal architecture of a protein kinase. *Biochim. Biophys. Acta* **2010**, *1804*, 440–4.
(19) Rabiller, M.; Getlik, M.; Kluter, S.; Richters, A.; Tuckmantel, S.; Simard, J. R.; Rauh, D. Proteus in the World of Proteins: Conformational Changes in Protein Kinases. *Arch. Pharm.* **2010**, *343*, 193–206.
(20) Gan, W.; Yang, S.; Roux, B. Atomistic View of the Conformational Activation of Src Kinase Using the String Method with Swarms-of-Trajectories. *Biophys. J.* **2009**, *97*, L8–L10.
(21) Zou, J.; Wang, Y. D.; Ma, F. X.; Xiang, M. L.; Shi, B.; Wei, Y. Q.; Yang, S. Y. Detailed conformational dynamics of juxtamembrane region and activation loop in c-Kit kinase activation process. *Proteins* **2008**, *72*, 323–332.
(22) Athanasios, P.; Dionisios, V.; Fotini, T.-S.; Michael, K. Conformational dynamics of the EGFR kinase domain reveals structural features involved in activation. *Proteins* **2009**, *76*, 375–386.
(23) Dixit, A.; Verkhivker, G. M. Hierarchical Modeling of Activation Mechanisms in the ABL and EGFR Kinase Domains: Thermodynamic and Mechanistic Catalysts of Kinase Activation by Cancer Mutations. *PLoS Comput. Biol.* **2009**, *5*, e1000487.
(24) Berteotti, A.; Cavalli, A.; Branduardi, D.; Gervasio, F. L.; Recanatini, M.; Parrinello, M. Protein Conformational Transitions: The Closure Mechanism of a Kinase Explored by Atomistic Simulations. *J. Am. Chem. Soc.* **2009**, *131*, 244–250.
(25) Shan, Y.; Seeliger, M. A.; Eastwood, M. P.; Frank, F.; Xu, H.; Jensen, M. O.; Dror, R. O.; Kuriyan, J.; Shaw, D. E. A conserved protonation-dependent switch controls drug binding in the Abl kinase. *Proc. Natl. Acad. Sci. U.S.A.* **2009**, *106*, 139–44.
(26) Ozkirimli, E.; Post, C. B. Src kinase activation: A switched electrostatic network. *Protein Sci.* **2006**, *15*, 1051–1062.
(27) Cheng, Y.; Zhang, Y.; McCammon, J. A. How does activation loop phosphorylation modulate catalytic activity in the cAMP-dependent protein kinase: A theoretical study. *Protein Sci.* **2006**, *15*, 672–683.
(28) Okuzumi, T.; Fiedler, D.; Zhang, C.; Gray, D. C.; Aizenstein, B.; Hoffman, R.; Shokat, K. M. Inhibitor hijacking of Akt activation. *Nat. Chem. Biol.* **2009**, *5*, 484–493.
(29) Yang, J.; Cron, P.; Good, V. M.; Thompson, V.; Hemmings, B. A.; Barford, D. Crystal structure of an activated Akt/Protein Kinase B ternary complex with GSK3-peptide and AMP-PNP. *Nat. Struct. Mol. Biol.* **2002**, *9*, 940–944.
(30) Brooks, B. R.; Brooks, C. L.; Mackerell, A. D.; Nilsson, L.; Petrella, R. J.; Roux, B.; Won, Y.; Archontis, G.; Bartels, C.; Boresch, S.; Caflisch, A.; Caves, L.; Cui, Q.; Dinner, A. R.; Feig, M.; Fischer, S.; Gao, J.; Hodoscek, M.; Im, W.; Kuczera, K.; Lazaridis, T.; Ma, J.; Ovchinnikov, V.; Paci, E.; Pastor, R. W.; Post, C. B.; Pu, J. Z.; Schaefer, M.; Tidor, B.; Venable, R. M.; Woodcock, H. L.; Wu, X.; Yang, W.; York, D. M.; Karplus, M. CHARMM: The Biomolecular Simulation Program. *J. Comput. Chem.* **2009**, *30*, 1545–1614.
(31) Gordon, J.; Myers, J.; Folta, T.; Shoja, V.; Heath, L.; Onufriev, A. H++: a server for estimating pKas and adding missing hydrogens to macromolecules. *Nucleic Acids Res.* **2005**, *33*, W368–371.
(32) Velin, Z. S.; Lisa, Y. A fast and accurate computational approach to protein ionization. *Protein Sci.* **2008**, *17*, 1955–1970.
(33) Li, H.; Robertson, A. D.; Jensen, J. H. Very fast empirical prediction and rationalization of protein pKa values. *Proteins* **2005**, *61*, 704–721.
(34) Glykos, N. M. Software news and updates. Carma: a molecular dynamics analysis program. *J. Comput. Chem.* **2006**, *27*, 1765–8.
(35) Tama, F.; Brooks, C. L. SYMMETRY, FORM, AND SHAPE: Guiding Principles for Robustness in Macromolecular Machines. *Annu. Rev. Biophys. Biomol. Struct.* **2006**, *35*, 115–133.
(36) Niv, M. Y.; Filizola, M. Influence of oligomerization on the dynamics of G-protein coupled receptors as assessed by normal mode analysis. *Proteins* **2008**, *71*, 575–86.
(37) Shudler, M.; Niv, M. Y. BlockMaster: Partitioning Protein Kinase Structures Using Normal-Mode Analysis. *J. Phys. Chem. A* **2009**, *113*, 7528–7534.
(38) Lindahl, E.; Azuara, C.; Koehl, P.; Delarue, M. NOMAD-Ref: visualization, deformation and refinement of macromolecular structures based on all-atom normal mode analysis. *Nucleic Acids Res.* **2006**, *34*, W52–56.
(39) Van Wynsberghe, A. W.; Cui, Q. Interpreting Correlated Motions Using Normal Mode Analysis. *Structure* **2006**, *14*, 1647–1653.
(40) Wang, Y. M.; Jernigan, R. L. Comparison of tRNA motions in the free and ribosomal bound structures. *Biophys. J.* **2005**, *89*, 3399–3409.
(41) Fiser, A.; Sali, A. ModLoop: automated modeling of loops in protein structures. *Bioinformatics* **2003**, *19*, 2500–2501.
(42) Hildebrand, P. W.; Goede, A.; Bauer, R. A.; Gruening, B.; Ismer, J.; Michalsky, E.; Preissner, R. SuperLooper-a prediction server for the modeling of loops in globular and membrane proteins. *Nucleic Acids Res.* **2009**, *37*, W571–W574.
(43) Stanton, C. L.; Houk, K. N. Benchmarking pKa Prediction Methods for Residues in Proteins. *J. Chem. Theory Comput.* **2008**, *4*, 951–966.
(44) Cox, S.; Taylor, S. S. Kinetic analysis of cAMP-dependent protein kinase: Mutations at histidine 87 affect peptide binding and pH dependence. *Biochemistry* **1995**, *34*, 16203–16209.
(45) Adams, J. A. Activation loop phosphorylation and catalysis in protein kinases: is there functional evidence for the autoinhibitor model. *Biochemistry* **2003**, *42*, 601–7.
(46) Hyeon, C.; Jennings, P. A.; Adams, J. A.; Onuchic, J. N. Ligand-induced global transitions in the catalytic domain of protein kinase A. *Proc. Natl. Acad. Sci. U.S.A.* **2009**, *106*, 3023–8.
(47) Na, Z.; Yongjun, J.; Jianwei, Z.; Qingsen, Y.; Wenna, Z. Structural basis for the complete loss of GSK3beta catalytic activity due to R96 mutation investigated by molecular dynamics study. *Proteins* **2009**, *75*, 671–681.
(48) Huang, X.; Begley, M.; Morgenstern, K. A.; Gu, Y.; Rose, P.; Zhao, H.; Zhu, X. Crystal structure of an inactive Akt2 kinase domain. *Structure* **2003**, *11*, 21–30.
(49) Amadei, A.; Linssen, A. B.; Berendsen, H. J. Essential dynamics of proteins. *Proteins* **1993**, *17*, 412–25.
(50) Amadei, A.; Ceruso, M. A.; Di Nola, A. On the convergence of the conformational coordinates basis set obtained by the essential dynamics analysis of proteins' molecular dynamics simulations. *Proteins* **1999**, *36*, 419–424.
(51) Humphrey, W.; Dalke, A.; Schulten, K. VMD: Visual molecular dynamics. *J. Mol. Graph.* **1996**, *14*, 33–38.
(52) Tama, F.; Sanejouand, Y. H. Conformational change of proteins arising from normal mode calculations. *Protein Eng.* **2001**, *14*, 1–6.
(53) Petrone, P.; Pande, V. S. Can conformational change be described by only a few normal modes. *Biophys. J.* **2006**, *90*, 1583–93.
(54) Niv, M. Y.; Skrabanek, L.; Filizola, M.; Weinstein, H. Modeling activated states of GPCRs: the rhodopsin template. *J. Comput.-Aided Mol. Des.* **2006**, *20*, 437–48.
(55) Tobi, D.; Bahar, I. Structural changes involved in protein binding correlate with intrinsic motions of proteins in the unbound state. *Proc. Natl. Acad. Sci. U.S.A.* **2005**, *102*, 18908–18913.
(56) Liu, Y.; Gray, N. S. Rational design of inhibitors that bind to inactive kinase conformations. *Nat. Chem. Biol.* **2006**, *2*, 358–364.
(57) Kufareva, I.; Abagyan, R. Type-II Kinase Inhibitor Docking, Screening, and Profiling Using Modified Structures of Active Kinase States. *J. Med. Chem.* **2008**, *51*, 7921–7932.
(58) Klepeis, J. L.; Lindorff-Larsen, K.; Dror, R. O.; Shaw, D. E. Long-timescale molecular dynamics simulations of protein structure and function. *Curr. Opin. Struct. Biol.* **2009**, *19*, 120–127.
(59) Kovacs, J. A.; Cavasotto, C. N.; Abagyan, R. Conformational sampling of protein flexibility in generalized coordinates: Application to ligand docking. *J. Comput. Theor. Nanosci.* **2005**, *2*, 354–361.
(60) May, A.; Zacharias, M. Protein-ligand docking accounting for receptor side chain and global flexibility in normal modes: Evaluation on kinase inhibitor cross docking. *J. Med. Chem.* **2008**, *51*, 3499–3506.
(61) Bakan, A.; Bahar, I. The intrinsic dynamics of enzymes plays a dominant role in determining the structural changes induced upon inhibitor binding. *Proc. Natl. Acad. Sci. U.S.A.* **2009**, *106*, 14349–14354.
(62) Essiz, S. G.; Coalson, R. D. A rigid-body Newtonian propagation scheme based on instantaneous decomposition into rotation and translation blocks. *J. Chem. Phys.* **2006**, *124*, 144116.
(63) Essiz, S. G.; Coalson, R. D. Langevin dynamics of molecules with internal rigid fragments in the harmonic regime. *J. Chem. Phys.* **2007**, *127*, 104109.
(64) Turjanski, A. G.; Hummer, G.; Gutkind, J. S. How Mitogen-Activated Protein Kinases Recognize and Phosphorylate Their Targets: A QM/MM Study. *J. Am. Chem. Soc.* **2009**, *131*, 6141–6148.
(65) Pettersen, E. F.; Goddard, T. D.; Huang, C. C.; Couch, G. S.; Greenblatt, D. M.; Meng, E. C.; Ferrin, T. E. UCSF Chimera--a visualization system for exploratory research and analysis. *J. Comput. Chem.* **2004**, *25*, 1605–12.

CI100076J